Synthesis of nanoparticles with femtosecond laser pulses

S. Eliezer,[1,*] N. Eliaz,[2] E. Grossman,[3] D. Fisher,[1,4] I. Gouzman,[3] Z. Henis,[1] S. Pecker,[1] Y. Horovitz,[1] M. Fraenkel,[1] S. Maman,[1] and Y. Lereah[5]

[1]*Plasma Physics Department, Soreq NRC, Yavne 81800, Israel*

[2]*Department of Solid Mechanics, Materials and Systems, Tel Aviv University, Ramat Aviv, Tel Aviv 69978, Israel*

[3]*Space Environment Division, Soreq NRC, Yavne 81800, Israel*

[4]*Faculty of Physics, Weizmann Institute of Science, Rehovot, 76100, Israel*

[5]*Wolfson Applied Materials Research Center, Tel Aviv University, Ramat Aviv, Tel Aviv 69978, Israel*

(Received 18 December 2003; published 23 April 2004)

First, a simple model describes theoretically the processes involved in the irradiation of solid targets by femtosecond laser pulses and predicts the optimal target and laser parameters for efficient nanoparticles synthesis. Then, we show experimental evidence for successful synthesis of aluminum nanoparticles. Nanoparticles size distribution, morphology, atomic structure, and chemical composition are determined by various techniques, including x-ray diffraction, atomic force microscopy, scanning and transmission electron microscopy, and energy dispersive spectroscopy.

DOI: 10.1103/PhysRevB.69.144119 PACS number(s): 52.50.Jm, 61.46.+w, 81.07.−b

I. INTRODUCTION

The synthesis and study of nanoparticles (NP's) of various elements and compounds is of great interest both for technological applications and for fundamental research. Traditionally, NP's have been produced by techniques such as arc discharge,[1] vapor deposition,[2] electrochemical deposition,[3] or ball milling.[4] In recent years, pulsed laser ablative deposition (PLD) has gained much interest for the production of thin films as well as NP's and their aggregates. PLD has several advantages over other processes, including the ability to produce materials with a complex stoichiometry and a narrower distribution of particle size, reduce porosity, and control the level of impurities.

Several papers provide experimental evidence for the production of thin films and NP's by means of PLD-based processes. Sturm *et al.*[5] studied the effect of an ambient Ar gas on the PLD of Ag and Fe films directly onto a microbalance, using an excimer KrF laser and a pulse width of 30 ns. Ullmann *et al.*[6] described the properties of nanosize aerosol particles generated by either reactive or nonreactive laser ablation of solid surfaces (pulse duration was about 28 ns). Pronko *et al.*[7] employed precisely controlled time-delayed secondary pulses for overcoming the plasma critical density limitations (namely, over dense or under dense). A Ti:sapphire laser producing pulses with energy up to 60 mJ and with pulse width of 60–150 fs was used. A plasma-jet nozzle effect was proposed to explain condensed cluster formation of Ge on Si at room temperature. Teghil *et al.*[8] used a Nd:glass laser with pulse duration of either 250 fs, 1.3 ps, or 6 ns to evaporate an $Al_{65}Cu_{23}Fe_{12}$ quasicrystalline target on an oriented Si substrate. The experimental analyses showed the presence of nanostructured films retaining the target stoichiometry but consisting of different crystalline and noncrystalline phases. The results also indicated that the ablation processes in the picosecond (ps) and femtosecond (fs) regimes are very different compared to the nanosecond one. Melting of the target during the ablation and a mechanism of material ejection was proposed for both the picosecond and femtosecond regimes. Wilson and Hamill[9] reported the synthesis of custom-engineered NP's via conversion of a feedstock into a high-temperature (50 000 K), high-pressure (100 atm) plasma, which was subsequently quenched to control the mean particle size. Dolbec *et al.*[10] deposited Pt NP's onto both highly oriented pyrolitic graphite (HOPG) and Si substrates. By varying the He background pressure and the target-to-substrate distance, a large range of kinetic energies could be obtained. The shape of the NP's was found to change from spherical at lower kinetic energies to flat at higher kinetic energies. The size of the NP's, however, was not dependent on the value of kinetic energy. Mao *et al.*[11] studied the mechanical properties of nanocrystalline Ni thin films prepared by PLD onto silica, sapphire or Ni substrates. Son *et al.*[12] performed parametric studies to suppress secondary phases in $LiNbO_3$ thin films prepared by PLD on sapphire and $LiNbO_3$. To this aim, a KrF excimer laser was used, with a pulse duration of 20 ns and laser fluence of $3-4\ J/cm^2$. From the references mentioned above it is evident that very little experimental work has been reported on the laboratory processing of NP's using ultrashort laser pulses.

In addition to these experimental investigations, several theoretical studies have suggested that rapid expansion and cooling of solid-density matter heated by a femtosecond laser pulse may result in NP synthesis via different mechanisms. Heterogeneous decomposition, liquid phase ejection and fragmentation, homogeneous nucleation and decomposition, spinodal decomposition, and photomechanical ejection may all lead to NP production in various target systems and under various heating regimes.[13–23] It is even possible that a considerable fraction of ejected material will be recovered in the form of amorphous or crystalline particles with radii ranging from 1 to 1000 nm.

The time scales of heating and cooling of target materials under fs laser pulses are significantly shorter than in the traditional NP synthesis processes. Expansion and decomposition of instantly heated solid-density targets have been studied theoretically for Lennard-Jones systems both in two

TABLE I. The average laser absorption coefficient (A), the laser irradiance (I_L), and the electron and ion temperatures (T_e and T_i, respectively) at various times and distances from the target/laser boundary for an aluminum target.

I_L (W/cm^2)	A	depth 10 nm time 100 fs		depth 10 nm time 1 ps		depth 50 nm time 100 fs		depth 50 nm time 5 ps	
		T_e (eV)	T_i (eV)	T_e (eV)	T_i (eV)	T_e (eV)	T_i (eV)	T_e (eV)	T_i (eV)
5.0×10^{12}	0.156	1.2	0.039	0.50	0.13	0.40	0.028	0.16	0.15
1.0×10^{13}	0.155	1.9	0.044	0.84	0.19	0.50	0.029	0.29	0.26
2.0×10^{13}	0.183	3.2	0.054	1.6	0.32	0.63	0.030	0.68	0.50
3.7×10^{13}	0.242	6.2	0.072	3.5	0.58	0.82	0.032	1.4	0.90
5.3×10^{13}	0.282	9.3	0.087	5.6	0.84	1.0	0.033	2.2	1.2
1.0×10^{14}	0.366	20	0.12	13	1.4	1.6	0.037	4.3	2.1
2.0×10^{14}	0.393	40	0.18	23	2.0	2.4	0.044	8.3	3.7

dimensions[14–16,18,19] and in three dimensions.[18,19,24] Mechanisms of ablation of a rapidly heated two-dimensional Lennard-Jones system were investigated by Perez and Lewis.[22,23] Ablation of graphite by femtosecond laser pulses was studied theoretically in Ref. 21, and detachment of monoatomic layers of carbon was predicted under some irradiation regimes. Ablation of silicon by femtosecond laser pulses was studied theoretically by Glover;[13] efficient production of NP's was predicted. Ablation of bulk aluminum (Al) by 500 fs, 1 μm laser pulse was studied theoretically by Vidal *et al.*[20] It was found that for peak laser intensities between 2×10^{12} and 2×10^{14} W/cm^2 the liquid phase comprised about 15% of the ejected mass.

The use of femtosecond lasers for NP's synthesis may be attractive for several reasons. First, because the pulse ends before expansion starts, the fs laser does not interact with the ejected material, thus allowing the study of the hydrodynamics and thermodynamics of the plasma expansion and of the NP formation without any external disturbances. Second, the fs laser pulses heat a material without changing its density, so that the initial thermodynamic conditions are easily known. Third, for a given laser fluence, the material is heated to a higher temperature and higher pressure compared to longer pulses because the laser is absorbed before any significant thermal conduction and plasma expansion take place. Therefore, the fs laser can heat any material to a solid-density plasma state with temperature and pressure above the critical point.

Hence, the goal of the present work is twofold. First, we model theoretically the processes involved in the irradiation of solid targets by femtosecond laser pulses and predict the optimal target and laser parameters for efficient NP's synthesis. The second goal is to verify experimentally the formation of NP's during irradiation of solid Al targets with femtosecond laser pulses and to fully characterize them. Aluminum targets are used in this work because both the optical properties and the equations of state (EOS) are well known for this metal. Moreover, highly crystalline Al NP's prepared by pulsed plasma have recently been reported[9] to produce more rapid and efficient burning of solid propellants than other existing powders. Thus, they are claimed to gain interest for applications in rocket fuels, high-energy explosives, and lead-free gun primers.

II. THEORETICAL PREDICTIONS

We have already reported elsewhere[25] the details of s-polarized fs laser absorption by Al targets. Here, however, we use p polarization at 45° incidences. Therefore, the Maxwell equations are solved directly instead of applying the Helmholtz equation as in Ref. 25. The electron and ion temperatures T_e and T_i, respectively, are calculated from the following energy conservation equations:

$$C_e(T_e)\frac{\partial T_e}{\partial t}=\frac{\partial}{\partial x}\left[\kappa(T_e)\frac{\partial T_e}{\partial x}\right]-U(T_e,T_i)+Q(x,t),$$

$$C_i(T_i)\frac{\partial T_i}{\partial t}=U(T_e,T_i), \tag{1}$$

where C_e and C_i are the electron and ion heat capacities, respectively, κ is the electron heat conductivity, U is the heat transfer rate from electrons to ions, t is time, x is the distance from the target surface inwards, and Q is the heat deposition rate due to the laser radiation absorption. The laser absorption changes significantly on scale of 10 nm, i.e., on the skin depth scale. As already mentioned, the laser energy deposition profile Q is rigorously determined by solving the appropriate Maxwell equations. The detailed expressions for C_e, C_i, and U are given in Ref. 25.

The absorption coefficient A is averaged over the laser temporal pulse profile $I(t)$ and is given by

$$I(t)=I_L\sin^2\left(\frac{\pi t}{2\tau_L}\right)\quad 0\leqslant t\leqslant 2\tau_L,\quad A=\frac{\int_0^{2\tau_L}dt\int_0^{\infty}Q(x,t)dx}{\int_0^{2\tau_L}I(t)dt}. \tag{2}$$

The results of these new calculations are summarized in Table I. As can be seen from this table, in the domain of 5×10^{12} to 2×10^{14} W/cm^2 approximately 15 to 40 % of the laser energy is absorbed. Results for T_e and T_i are also summarized in Table I.

The solution of the above equations at equilibrium ($T_e=T_i$) defines the initial conditions for the adiabatic plasma expansion. For the adiabatic expansion of the dense plasma we apply our EOS (see, for example, Ref. 26), which is practically the wide-range semi-empirical EOS described in

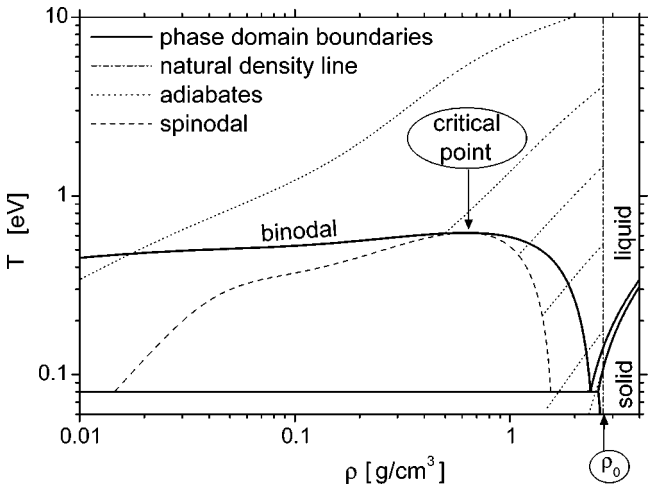

FIG. 1. Phase diagram of aluminum. Solid lines show phase domain boundaries, the dashed line shows the spinodal decomposition, dotted lines show adiabatic expansion paths for various T_0 values ($\rho_0 = 2.7$ g/cm^3).

detail in Ref. 27. Detailed calculations are performed for T_e and T_i at various depths and times before the expansion onset, as a function of the peak intensity I_L at that location on the target surface. Laser spot size is large enough ($\sim$ few mm) to neglect tangential heat exchange. The data on temperature is used to locate the initial point on the phase diagram for the adiabatic expansion (AE) of the irradiated material. On the (ρ,T) diagram, each element of the target material starts its AE at the same density ρ_0 (natural density of the material) but at a different initial temperature T_0.

The ultrashort pulse allows completing the energy deposition into the target well before the target expansion begins and effectively decoupling these two stages of the process. The radiation energy is initially deposited in the electron subsystem, within a target surface layer of few tens of nm thick. After the pulse ends, but before the hydrodynamic expansion sets in, the electrons in the surface layer undergo cooling by heat diffusion and by heat transfer to ions (phonons). This stage continues for several picoseconds. Next, the expansion starts, and consequently the heat transfer gradually ceases, making the expansion adiabatic. According to our EOS, the rarefaction wave front velocity (sound velocity) in solid-density Al is 5.4 nm/ps at room temperature[28] and 13 nm/ps at a temperature of $T=(T_e=T_i)=11$ eV. This implies that the rarefaction at 10 nm depth starts roughly 1 picosecond after the pulse, and at 50 nm depth—between 5 and 9 ps after the pulse.

The (ρ,T) diagram of Al is presented in Fig. 1. AE paths for various T_0 traverse different regions of the diagram. Paths starting at $T_0=3-4$ eV reach the binodal in the critical point vicinity; paths starting at higher T_0 pass above the critical point. Paths starting at $T_0>20$ eV never reach the binodal. This corresponds to material that is converted into plasma, expands, cools, recombines into gas, and is eventually deposited on the vacuum vessel walls as individual atoms. Paths starting at $T_0\approx 8-20$ eV reach the binodal at subcritical densities, but never reach the spinodal. Paths starting at $T_0\approx 4-8$ eV reach the spinodal at subcritical densities.

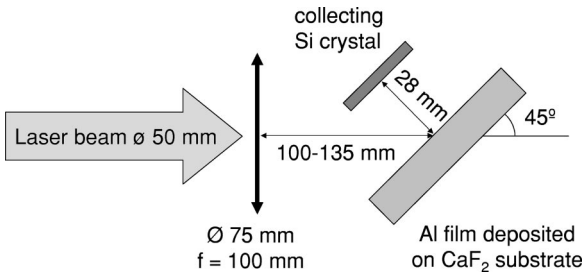

FIG. 2. Schematics of the experimental setup and conditions.

Some NP's can thus form, especially at lower T_0 (close to 4 eV). Paths starting at $T_0\approx 0.2-4$ eV are the most promising in the context of NP production, as they reach the spinodal at supercritical or near-critical densities; as phase decomposition occurs, a relatively large fraction of the material assumes a liquid state. Of course, the higher is T_0, the more the NP size distribution shifts towards smaller NP sizes. Paths starting at $T_0\leqslant 0.18$ eV do not reach the spinodal and describe a material that either remains unevacuated or leaves the target as droplets of liquid. These paths do not contribute to NP production.

The above considerations are valid for the regions of the target that, by the time rarefaction starts affecting them, can be described, at least approximately, by a single temperature. This is the case for the entire target except a surface layer about 10 nm thick. Furthermore, for laser irradiances larger than 10^{14} W/cm^2, the electrons and the ions start to expand before reaching equilibrium. In this case one has a double-temperature adiabatic expansion[29] of electron and ion plasmas. In this case the relevant ion temperature is smaller than the appropriate temperature at 10^{13} W/cm^2 and, therefore, larger NP's are created. Based on the above analysis, the most effective NP production is expected for $I_L\sim 5\times 10^{13}$ W/cm^2.

III. EXPERIMENTAL PROCEDURES AND RESULTS

Upon completion of the first part of the work in which the fundamental processes and conditions for efficient NP's production have been defined, experimental study is carried out to support the theoretical findings. In the present work a Ti:sapphire laser beam, with 50 fs pulse duration, 0.8 μm wavelength and a diameter of few millimeters, irradiates a target. The spatial laser intensity profile is Gaussian to a good approximation. The target here is a 100 nm thick Al foil on a transparent heat-insulating CaF_2 glass substrate. The pressure in the vacuum chamber is 10^{-4} Torr. The laser irradiates the target at an angle of 45° and with intensities varying between 3×10^{12} W/cm^2 and 5×10^{14} W/cm^2. Experimental conditions are summarized in Fig. 2. The heated plasma expands into the vacuum perpendicular to the Al target, whereas the debris are collected either on a silicon wafer [for x-ray diffraction (XRD), scanning electron microscopy (SEM), and atomic force microscopy (AFM)] or on a copper grid covered on one side with a carbon membrane [for transmission electron microscopy (TEM)].

Visual examination of either the wafer or the grid follow-

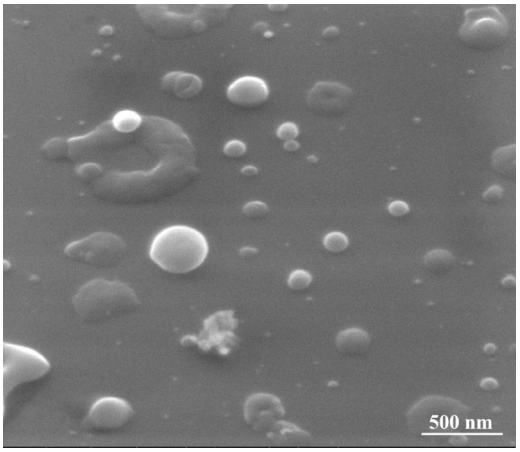

FIG. 3. Scanning electron microscope image of mainly spherical nanoparticles deposited onto a silicon substrate.

ing the irradiation experiments reveals the existence of a white nondense deposit. The atomic structure of this deposit on a silicon wafer is determined by XRD (a Θ-Θ powder diffractometer). Through comparison to the JCPDS (Joint Committee on Powder Diffraction Standards) file for the cubic Al phase (No. 04-0787), it becomes apparent that a separate phase of pure crystalline Al has formed on the surface. However, a shift of the reflections to slightly lower angles indicates that compressive stresses were probably introduced to the deposit. The same XRD data also allows calculation of a lattice parameter which is slightly larger in the z direction (4.0700 ± 0.0045 Å) and smaller in the x and y directions compared to the lattice parameter given in JCPDS No. 04-0787 (4.0494 Å). It should be noted that in order for the light Al to be detectable by XRD, the deposit should be thick enough. In addition, the XRD spectrum is basically obtained as an average of different particles.

SEM micrographs revealing a general view of the Al particles-deposited wafer are also obtained. Figure 3 shows the spherical shape of selected Al particles. In general, both the size and the shape of the deposited particles are observed to be widely distributed, the former ranging from tens nanometers to as high as approximately 500 nm. Chemical composition of the deposited particles is also assessed in the SEM by means of energy dispersive x-ray spectroscopy (EDS). Silicon and Al from the substrate and deposited particles, respectively, are detected. AFM provides near-atomic resolution and is therefore used here to study small NP's. Measurements are carried out using a Digital Instruments Nanoscope II system with a 140 μm scanner, operating in the height mode under ambient conditions. Figure 4 shows an AFM image of particles deposited onto Si substrate. This image reveals particles ranging from 10 to 50 nm in diameter

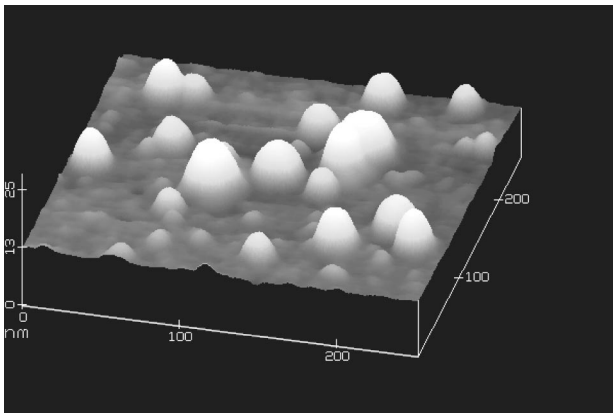

FIG. 4. Atomic force microscope image of nanoparticles deposited onto a silicon substrate. Scan size is 250×250 nm, the z range is 25 nm.

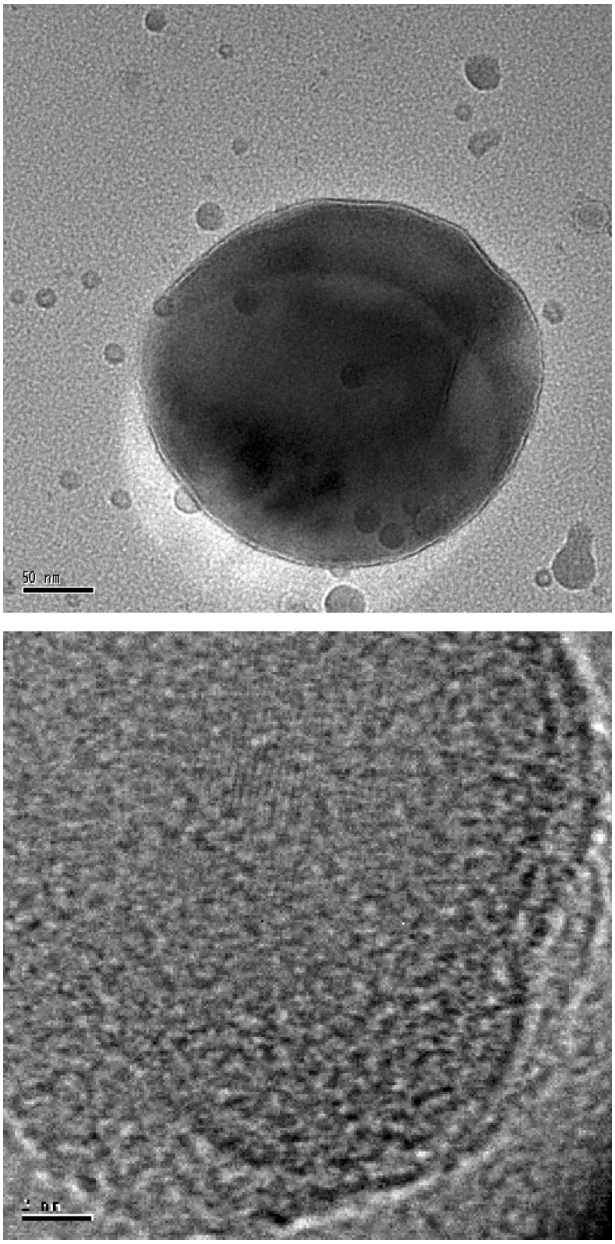

FIG. 5. Transmission electron microscope bright-field images of aluminum nanoparticles deposited onto a copper grid covered with an amorphous carbon membrane. (a) Low magnification showing a group of spherical nanoparticles smaller than 50 nm. (b) High-resolution image showing arrays of atoms that illustrate the crystalline structure of this 24-nm-size nanoparticle.

and from 2 to 10 nm in height.

The size distribution of the NP's is determined with the aid of an image analysis software package based on the AFM data. The cumulative number density $f(S)$ of NP's (from infinity to S) as measured by the AFM is found to fit well to the following formula:

$$f(S)[\text{particles}/\mu\text{m}^2] = \alpha_1 \exp\left(-\frac{S}{\mu_1}\right) + \alpha_2 \exp\left(-\frac{S}{\mu_2}\right), \tag{3}$$

where S is the area of the measured NP in units of nm^2 and α_1, α_2, μ_1, and μ_2 are constants. For example, with a laser irradiance of 3.7×10^{13} W/cm^2 we get $\alpha_1 = 121\ \mu\text{m}^{-2}$, $\alpha_2 = 190\ \mu\text{m}^{-2}$, $\mu_1 = 827\ \text{nm}^2$, and $\mu_2 = 168\ \text{nm}^2$. The diameter of the NP's layer on the silicon substrate is about 3 mm; the NP's distribution across this layer is homogeneous to a good approximation. The total number of particles per unit area, N, and the average dimension $\langle S\rangle$ of NP's are expressed [using Eq. (3)] as

$$N(\text{particles}/\mu\text{m}^2) = f(0) = \alpha_1 + \alpha_2,$$

$$\langle S\rangle = \frac{\int_0^\infty S\frac{df}{dS}dS}{\int_0^\infty \frac{df}{dS}dS} = \frac{\alpha_1\mu_1 + \alpha_2\mu_2}{\alpha_1 + \alpha_2}. \tag{4}$$

Our experiments give $N = 4$, 300, 1000, and 30 particles/μm^2 for $I_L = 3\times10^{12}$, 3.7×10^{13}, 5.3×10^{13}, and 5×10^{14} W/cm^2, respectively. For the same laser irradiances we get appropriately $\langle S\rangle = 1.2\times10^4$, 4.2×10^2, 1.2×10^2, and 5×10^3 nm^2. Note that the total number of particles per unit area significantly decreases at the highest laser irradiance because the initial temperature (before the adiabatic expansion) is too high (see Fig. 1). Moreover, at higher laser irradiances no NP's formation is observed. The experimental values are thus in good agreement with the qualitative model described above.

TEM is also used here to characterize the structure and the composition at a subnanometer resolution of the NP's deposited onto the copper grid. A Philips Tecnai F20 microscope (a field emission gun microscope operating at 200 kV), equipped with an EDS detector from EDAX for chemical analysis, is used. Representative results from an in depth study are given herein. TEM micrographs reveal once again the large distribution in NP's size, from less than 10 nm to hundreds of nanometers. Figure 5(a) is a bright-field image showing a group of NP's with diameters smaller than 50 nm. The largest dark circle seems to cover itself a group of NP's. Figure 5(b) is a high-resolution bright-field image of a particle approximately 24 nm in diameter. Line arrays of atoms may be noted, indicating the crystalline nature of this particle. It should be noted that in various regions of this and other particles no atom planes can be identified. This may indicate that, at least in some particles, both amorphous and nanocrystalline structures of Al coexist. EDS analysis from the vicinity of the particle shown in Fig. 5(b) reveals a high Al peak, together with peaks of copper and carbon (from the grid) as well as oxygen. Fast Fourier transform (FFT) and electron diffraction from particles deposited onto the copper grid typically do not provide in this work nice diffraction patterns due to the encapsulation of the light nanocrystalline Al particles in the folded amorphous carbon membrane and the absence of good Bragg conditions. Yet, two clear spots are observed in the diffraction pattern of the particle shown in Fig. 5(b). The distance between these spots is found to be 2.354 ± 0.118 Å, which is in good agreement with the strongest reflection from the cubic Al phase (2.338 Å for planes {111} according to JCPDS No. 04-0787).

IV. DISCUSSION AND CONCLUSIONS

It is shown in this paper that while keeping the Al source and the Si substrate the same for all experiments, the NP's production changes only with laser parameters; namely, for equivalent substrate temperature, impurities and surface roughness, the particles number and size depend only on the plasma parameters, which in turn are a function of the laser irradiance for a given target. In particular, the number of NP's changes with the laser irradiance I_L quite drastically. At laser irradiances lower than 3×10^{12} W/cm^2 or higher than 5×10^{14} W/cm^2 no NP's formation is observed. Furthermore, similar NP's form either on a silicon wafer substrate or on a copper grid covered with carbon, and the Al deposit is thick enough to be detected by XRD. Hence, it is conceivable to conclude that these observations indicate that the particle formation as described in this work is a gas phase process and is not dependent on the substrate nature.

To conclude, this work provides calculation of the initial conditions, created by a femtosecond laser plasma interaction, for an adiabatic expansion of the plasma and the creation of nanoparticles. Subsequently, it describes the first experimental evidence for the synthesis of aluminum nanoparticles and their characterization. The next step should be to optimize the process so that the nanoparticles shape and size distribution can be better controlled in a reproducible manner.

ACKNOWLEDGMENTS

The authors acknowledge the very important contribution of Dr. Arie Borowitz at the early stages of this research. Useful discussions with Professor Arie Zigler are greatly appreciated.

*Electronic address: eliezer@soreq.gov.il

[1] Yu.E. Lozovik and A.M. Popov, Mol. Mater. **7**, 89 (1996).

[2] S.L. Stoll, E.G. Gillan, and A.R. Barron, Chem. Vap. Deposition **2**, 182 (1996).

[3] S. Banerjee, S. Roy, J.W. Chen, and D. Chakravorty, J. Magn. Magn. Mater. **219**, 45 (2000).

[4] W. Abdul-Razzaq and M.S. Seehra, Phys. Status Solidi A **193**, 94 (2002).

[5] K. Sturm, S. Fähler, and H.-U. Krebs, Appl. Surf. Sci. **154–155**, 462 (2000).
[6] M. Ullmann, S.K. Friedlander, and A. Schmidt-Ott, J. Nanopart. Res. **4**, 499 (2002).
[7] P.P. Pronko, Z. Zhang, and P.A. VanRompay, Appl. Surf. Sci. **208–209**, 492 (2003).
[8] R. Teghil, L. D'Alessio, A. Santagata, M. Zaccagnino, D. Ferro, and D.J. Sordelet, Appl. Surf. Sci. **210**, 307 (2003).
[9] D. Wilson and D. Hamill (unpublished).
[10] R. Dolbec, E. Irissou, F. Rosei, D. Guay, M. Chaker, and M. El Khakani (unpublished).
[11] S. Mao, Z. Shan, and J. Knapp (unpublished).
[12] J. Son, S. Orlov, B. Phillips, and L. Hesselink (unpublished).
[13] T.E. Glover, J. Opt. Soc. Am. B **20**, 125 (2003).
[14] F.F. Abraham, S.W. Koch, and R.C. Desai, Phys. Rev. Lett. **49**, 923 (1982).
[15] J.A. Blink and W.G. Hoover, Phys. Rev. A **32**, 1027 (1985).
[16] B.L. Holian and D.E. Grady, Phys. Rev. Lett. **60**, 1355 (1988).
[17] K. Sokolowski-Tinten, J. Bialkowski, A. Cavalleri, D. von der Linde, A. Oparin, J. Meyerter-Vehn, and S.I. Anisimov, Phys. Rev. Lett. **81**, 224 (1998).
[18] S. Toxvaerd, Phys. Rev. E **58**, 704 (1998).
[19] Wm.T. Ashurst and B.L. Holian, Phys. Rev. E **59**, 6742 (1999).
[20] F. Vidal, T.W. Johnston, S. Laville, O. Barthelemy, M. Chaker, B. Le Drogoff, J. Margot, and M. Sabsabi, Phys. Rev. Lett. **86**, 2573 (2001).
[21] H.O. Jeschke, M.E. Garcia, and K.H. Bennemann, Phys. Rev. Lett. **87**, 015003 (2001).
[22] D. Perez and L.J. Lewis, Phys. Rev. Lett. **89**, 255504 (2002).
[23] D. Perez and L.J. Lewis, Phys. Rev. B **67**, 184102 (2003).
[24] S.I. Anisimov, D.O. Dunikov, V.V. Zhakhovskii, and S.P. Malyshenko, J. Chem. Phys. **110**, 8722 (1999).
[25] D. Fisher, M. Fraenkel, Z. Henis, E. Moshe, and S. Eliezer, Phys. Rev. E **65**, 016409 (2001).
[26] E. Moshe, S. Eliezer, Z. Henis, M. Werdiger, E. Dekel, Y. Horovitz, S. Maman, I.B. Goldberg, and D. Eliezer, Appl. Phys. Lett. **76**, 1555 (2000).
[27] A.V. Bushman, G.I. Kanel, A.L. Ni, and V.E. Fortov, *Intense Dynamic Loading of Condensed Matter* (Taylor & Francis, London, 1993). The EOS proper is provided in Chap. 8.
[28] S. Eliezer, A. Ghatak, and H. Hora, *Fundamentals of Equations of State* (World Scientific, New Jersey, 2002).
[29] S. Eliezer, *The Interaction of High-Power Lasers with Plasmas* (Institute of Physics, Bristol, 2002).